Journal of Orthopaedic Translation 31 (2021) 52–61

Contents lists available at ScienceDirect

Journal of Orthopaedic Translation

journal homepage: www.journals.elsevier.com/journal-of-orthopaedic-translation

Original Article

NF-κB activation impedes the transdifferentiation of hypertrophic chondrocytes at the growth plate of mouse embryos in diabetic pregnancy

Xi Liu [a,1], Fan Qian [a,1], Qiwei Fan [a], Li Lin [a], Meiyao He [a], Peizhi Li [a], Hongmei Cai [a], Lisha Ma [a], Xin Cheng [a,b,**], Xuesong Yang [a,b,*]

[a] Division of Histology and Embryology, International Joint Laboratory for Embryonic Development & Prenatal Medicine, Medical College, Jinan University, Guangzhou, 510632, China
[b] Key Laboratory for Regenerative Medicine of the Ministry of Education, Jinan University, Guangzhou, 510632, China

ARTICLE INFO

Keywords:
Diabetes mellitus
Endochondral bone formation
Growth plate
Hypertrophic zone
NF-κB signaling
bone morphogenetic protein 2, Bmp2

ABSTRACT

Background: Diabetes mellitus could cause numerous complications and health problems including abnormality of endochondral bone formation during embryogenesis. However, the underlying mechanisms still remain obscure.
Methods: Streptozotoci (STZ) was injected to induce pregestational diabetes mellitus (PGDM) mouse model. The femurs of E18.5 mouse embryos from control and PGDM groups were harvested. Morphological staining was implemented to determine the abnormality of the bone development. The expressions of the key genes participating in osteogenesis (e.g., Sox9, Runx2, and Osterix), the NF-κB signaling molecules (e.g., P50, P65, IκBα), and the corresponding regulatory factors (e.g., Bmp2, phospho-p38) were evaluated by immunofluorescence, quantitative PCR and western blot. Finally, in vitro chondrocyte differentiation model was employed to verify the role of NF-κB on the expressions of chondro-osteogenic markers.
Results: Alcian blue/alizarin red double staining and H&E staining demonstrated the restriction of skeletal development and relatively extended hypertrophic zone at growth plate in E18.5 STZ-induced diabetic mouse embryos compared to the control. Immunofluorescent staining and qPCR showed that Sox9 expression increased, while Runx2 and Osterix expressions decreased in the growth plate of the offspring of PGDM mice. Immunofluorescence of P65 manifested the activation of NF-κB signaling in growth plate in PGDM mouse embryos. Furthermore, the relatively extended hypertrophic zone was also observed in the growth plate of the NF-κB-activated transgenic mice, as well as the activated p65 up-regulated the expression of Bmp2 and p-p38. In ATDC5 cells, we could observe the high glucose up-regulated the P50 and P65 expressions and down-regulated IκBα expression, but the high glucose-activated NF-κB signaling could be reversed by addition of Bay (inhibitor of NF-κB signaling). The expression changes of Bmp2, Sox9 and Runx2 in presence of high glucose were resumed too.
Conclusion: Our data revealed that NF-κB signaling was involved in mediation effects of dysfunctional transdifferentiation of hypertrophic chondrocytes in the embryonic growth plate induced by maternal diabetic mellitus.

1. Introduction

In the new century, diabetes mellitus has been becoming one of the overwhelming issues facing health care in the world [1]. Diabetes is deemed to be a disorder that influences on burning food into energy in the human body. There are three kinds of diabetes mellitus: type 1 (T1DM), type 2 (T2DM), and gestational diabetes (GDM) [2–4]. T1DM refers to the problems manufacturing insulin; T2DM refers to the problems using insulin well; gestational diabetes is the diabetes mellitus diagnosed during pregnancy [3]. Women affected by diabetes in pregnancy fall into 1 of 2 broad diagnostic categories – pregestational gestational diabetes mellitus (PGDM, including T1DM and T2DM) and

* Corresponding author. Division of Histology and Embryology, International Joint Laboratory for Embryonic Development & Prenatal Medicine, Medical College, Jinan University, Guangzhou, 510632, China.
** Corresponding author. Division of Histology and Embryology, International Joint Laboratory for Embryonic Development & Prenatal Medicine, Medical College, Jinan University, Guangzhou, 510632, China.
E-mail addresses: tchengxin@jnu.edu.cn (X. Cheng), yang_xuesong@126.com (X. Yang).
[1] Contribute to the work equally

https://doi.org/10.1016/j.jot.2021.10.009
Received 22 July 2021; Received in revised form 25 October 2021; Accepted 28 October 2021

gestational diabetes mellitus (GDM). The International Diabetes Federation (IDF) suggests that 16.8% pregnancies are affected by diabetes. Of this number, 13.6% are affected by PGDM, and this proportion keep increasing in recent years [5]. It has been known that diabetes mellitus is associated with various fetal and infant complications, such as stillbirth, prenatal mortality, infant macrosomia and birth trauma, infant hypoglycemia [6–9], and most of the underlying pathological mechanisms have not been completely understood.

Both T1DM and T2DM have been reported to interfere with developmental osteogenesis and impair fracture healing [10,11], but the pertinent data regarding the influence of diabetes mellitus on embryonic/fetal bone formation have not been well elucidated. As we know, multifactorial interventions such as the external influence (e.g., maternal diabetes) of various genes, growth factors and enzymes would contribute to the inadequate embryogenesis including the underdevelopment of the skeletal system. Our previous experiments showed that the high glucose could negatively affect the skeletal development of chick embryos through Wnt signaling [12]. Moreover, another report displayed that there was a significant inverse correlation between the fetal bone mineral content and the blood glucose of diabetic mothers in the first trimester, i.e., low neonatal bone mineral content is associated with high maternal blood glucose [13]. In addition, gestational diabetes could result in different degrees of limb deformities and underdevelopment of the fetus [14,15]. More importantly, the inappropriate skeletal development during fetal period or childhood could directly affect the morbidity of the systematic skeletal disorders in adulthood (e.g., osteoporosis), since the pathology of skeletal development roots in fetal/neonatal bone health [16]. In the view of the importance of this problem, we systematically implemented the study about the effects of maternal diabetes on the long bone formation in the stage of embryonic development.

The development and growth of long bones are accomplished by means of endochondral ossification, in which the chondrocytes form a template of hyaline cartilage and then the cartilaginous template is gradually replaced by bone, with blood vessels invasion, and matrix ossification. In recent years, a new theory about the cell fate of chondrocytes in endochondral bone formation has been summarized [17]. That is the direct cell transdifferentiation from chondrocytes to bone cells precisely connects chondrogenesis, classified as phase I, providing a template of the future skeleton. The chondrocytes go through cell proliferation and hypertrophic differentiation to form a distinctive growth plate, where chondrocytes on the epiphyseal plate divide into one cell remaining undifferentiated near the epiphysis, and another cell moving toward the diaphysis which continuously pushes longitudinal bone growth [18]. In growth plate, newly-formed round shaped chondrocytes morphologically become flat, and eventually diminish proliferative feature and exit the cell cycle to enter the prehypertrophic phase. Phase II is classified as osteogenesis, which finishes skeletal construction [17]. Hypertrophic chondrocytes facilitate the mineralization of the surrounding matrix, tempt the invasion of blood vessels via secreting vascular endothelial growth factor (VEGF), and then macrophage-derived osteoclasts break down the existing cartilage matrix. Meanwhile, osteoblasts derived from the adjacent perichondrium of hypertrophic zone, synthesize bone matrix to form a bone collar [18]. These two phases are in a continuous lineage-linked process of endochondral bone formation and limb elongation.

The process of the cell transdifferentiation in the growth plate during the relay from chondrogenesis to osteogenesis is coordinately controlled by many local paracrine regulators and endocrine hormones, such as bone morphogenetic proteins (BMPs), fibroblast growth factors (FGFs), insulin-like growth factors (IGFs), retinoids and the parathyroid hormone-related protein (PTHrP)/Indian hedgehog (Ihh) signaling loop [18–23]. Among these factors, Bmp2, a member of the TGF-β super-family, plays an essential role in the regulation of chondrocyte proliferation and maturation during endochondral bone development [24]. Bmp2 shows a tremendous potential to induce chondrogenesis, osteogenic differentiation [25], and endochondral ossification [24]. Bmp2 can induce chondrogenic and osteogenic differentiation within the same system, implying the essential role of Bmp2 during bone development and cartilage/bone regeneration. P38 kinase is stimulated by Bmp2 and functions as the downstream signal [26,27]. Bmp2 activates MAP kinase, and consequently elicits MKK3/MKK6 that directly phosphorylates and activates p38 kinase [27–29]. The phosphorylated p38 kinase, in turn, regulates gene expression in the nucleus.

It is reported that nuclear factor kappa B (NF-κB) specifically activates Bmp2 expression in chondrocytes, which implies that NF-κB is the upstream signaling of Bmp2 [30]. NF-κB signaling has been judged to fully exploit its indispensable role in the immune system through regulating and inducing the expressions of highly effective genes in the body in responses to internal and external pathogens [31]. However, the transcriptional regulation of NF-κB signaling is far beyond the immune responses to pathogens, actually extending to influence on cell survival, proliferation and differentiation [31]. The basic forms of NF-κB signaling comprise receptor and adaptor molecules, IKK complex, IκB proteins and NF-κB dimmers, while NF-κB family of the transcription factors includes the following five members: p50, p52, p65 (RelA), c-Rel, and RelB [32,33]. The activation of NF-κB transcription is fulfilled through the release of NF-κB dimmer, e.g., phosphorylation of p65, which interacts with CBP/p300 coactivator complexes resulting in target gene transcription [33].

In this study, diabetic mouse model and the ATDC5 (chondrogenic cell line) cells were employed to investigate the effect of maternal diabetes on fetal chondrogenesis and osteogenesis, as well as the pathological mechanism including the involvement of NF-κB signaling.

2. Materials and methods

2.1. Mouse embryos

The C57BL/6 mice used in this study were obtained from the Institute of Laboratory Animal Science, Jinan University (Guangzhou, China). Eight-week old female mice were used to induce diabetes mellitus by injecting 2% streptozotocin (STZ, Sigma, MO, USA) dissolved in 0.01 M citrate buffer at a pH of 4.5 and a dose of 75 mg/kg body weight for 3 consecutive days. Blood glucose levels were measured 7 days after STZ injection by Roche Accu-Chek Aviva Blood Glucose System (Roche, USA). Diabetes mellitus was defined as a fasting blood glucose level greater than 288 mg/dL (16 mM) [1,2]. Control mice were maintained euglycemic prior to and during pregnancy (4–8 mM). Two female mice were housed with one normal male mouse overnight in a cage. The day that vaginal plugs were observed was designated as embryonic day 0.5 (E0.5). During pregnancy, blood glucose levels were monitored every 6 days. The fetuses were dissected by caesarean section after the pregnant mice were anaesthetized by injecting pentobarbital (150 mg/kg body weight) at E18.5, which is corresponding to 6 months of human fetal developmental stage, the time point representing the key stage of endochondral ossification. The experiments were performed in duplicate, with 24 mice randomly assigned to control and PGDM group, respectively. All processes involving animal treatments in this study were in accordance with the procedures of Ethical Committee for Animal Experimentation, Jinan University.

2.2. NF-κB1^{C59S} mice

Knockin (NF-κB1^{C59S}) mice were obtained from Modern Animal Research Center of Nanjing University. NF-κB1^{C59S} mice (activated NF-κB) were established as previously reported [34]. The knee joints of the 1 month NF-κB1^{C59S} mice were harvested for sectioning, stained with 0.1% safranin O (Sigma, USA) and 0.1% fast green (Sigma, USA). All processes involving animal treatments in this study were in accordance with the procedures of Ethical Committee for Animal Experimentation, Jinan University.

Table 1
PCR primer.

Gene	Primer	Sequence
(M)Sox9	Forward	5′-AGACTCACATCTCTCCTAATGCT-3′
	Reverse	5′-ACGTCGGTTTTGGGAGTGG-3′
(M)Runx2	Forward	5′-CTCTTCTGGAGCCGTTTATGT-3′
	Reverse	5′-GTTTCTTAGGGTCTTGGAGTGA-3′
(M)Osterix/SP7	Forward	5′-ACCCCAAGATGTCTATAAGCCC-3′
	Reverse	5′-CGCTCTAGCTCCTGACAGTTG-3′
(M)Bmp2	Forward	5′-GGGACCCGCTGTCTTCTAGT-3′
	Reverse	5′-TCAACTCAAATTCGCTGAGGAC-3′
(M)p50	Forward	5′-TCGCTCAGCTGCACTCTATG-3′
	Reverse	5′-GGGGACAGCGACACCTTTTA-3′
(M)p65	Forward	5′-ACCCTGACCATGGACGATCT-3′
	Reverse	5′-CCCCTCGCATTTATAGCGGA-3′
(M) IκBα	Forward	5′-AGGTGATTTTCCAGAACCTAATGAA-3′
	Reverse	5′-CAAGAAGGCGACACAGACCT-3′
(M)β-actin	Forward	5′-GTGCTATGTTGCTCTAGACTTCG-3′
	Reverse	5′-ATGCCACAGGATTCCATACC-3′

2.3. Alcian blue and alizarin red staining

To visualize the skeleton, the whole mouse embryos were stained with alcian blue and alizarin red dyes as previously described [35]. The mouse embryos were separated from adherent tissues, fixed in 95% ethanol for 2 days followed by fixation in acetone for another additional day, stained for cartilage with alcian blue and counterstained for bone with alizarin red (Solarbio, Beijing, China). Long bone tissues were carefully dismembered and photographed using a stereomicroscope (MVX10, Olympus, Tokyo, Japan). The lengths of each humerus, ulna, radius, femur, fibula and tibia were quantitatively analyzed using Image Pro-Plus 5.0 software (IPP, Media Cybernetics) [36].

2.4. Cell culture

Chondrogenic cell line ATDC5 (ATCC, Manassas, VA) cells were cultured in Dulbecco's Modified Eagle Medium (DMEM, Gibco) and plated with a density of 1×10^6 cells/mL, supplemented with 10% fetal bovine serum (FBS, Gibco, Gaithersburg, MD). The chondrogenic differentiation medium was supplemented with insulin-transferring-sodium selenite media supplement (Sigma) for 4 days. The cultures were exposed to 25 mM (normal) or 50 mM (high glucose) D-glucose (Sigma, MO, USA), while 50 mM mannitol was used as osmotic control in order to determine whether or not the effect of high glucose was related to the osmotic effect. To address the possible role of NF-κB signals, the ATDC5 cells cultured with either 25 or 50 mM D-glucose were treated with 5 μM Bay-117082 (NF-κB inhibitor, Thermo Fisher Scientific, USA).

2.5. H&E staining, von Kossa staining and immunofluorescent staining

The femurs of the mouse embryos from control and STZ-treated groups were dismembered and fixed in 4% paraformaldehyde (PFA), then embedded in paraffin. The samples were serially sectioned at 5 μm thicknesses on a microtome (Leica RM2126RT, Germany). Bone histology analyses including H&E staining and von Kossa staining were performed with longitudinal sections using standard protocols. Immunofluorescent staining was performed at 4 °C overnight, using

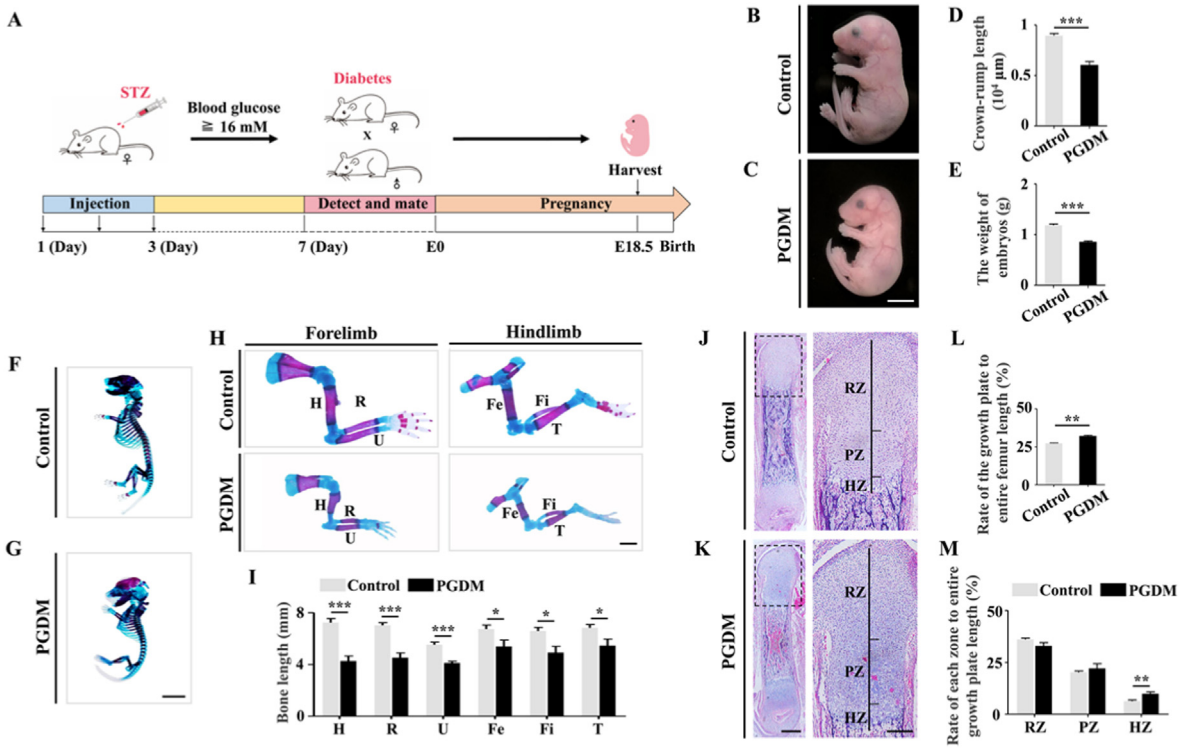

Fig. 1. Assessing the long bone formation of mouse embryos from control and PGDM group. **A**: Sketch illustrating the establishment of STZ-induced PGDM mouse model and the timing for harvesting mouse embryos. **B-E**: Representative bright-field images of E18.5 mouse embryos from control (B) and PGDM (C) group. Bar charts showing the comparisons of crown-rump length (D) and weight (E) of E18.5 mouse embryos from control and PGDM groups. **F–H**: Representative alcian blue/alizarin red stained images of E18.5 mouse embryos from control (F) and PGDM (G) groups. High magnification images of forelimb and hindlimb (H) from the two groups. **I**: Bar charts showing the length comparisons of humerus (H), radius (R), ulna (U), femur (Fe), fibula (Fi) and tibia (T) of E18.5 mouse embryos from control and PGDM groups. **J-K**: Representative H&E stained images of vertical sections of femurs from E18.5 control (J) and PGDM (K) mouse embryos. Right panels show the high magnification images indicated by dotted squares in left panels. **L-M**: Bar charts showing the ratios comparisons of growth plate length to the entire femur (L) and the ratios of RZ (reserve zone), PZ (proliferative zone) and HZ (hypertrophic zone) length (M) to the entire growth plate of E18.5 mouse embryos from control and PGDM groups. Scale bars = 5 mm in B–C and F-G; 2000 μm in H; 400 μm in the left panels of J-K, 200 μm in the right panels of J-K. For D, I and L, n = 6, for E, n = 10, for M, n = 5. $^*P < 0.05$, $^{**}P < 0.01$, $^{***}P < 0.001$.

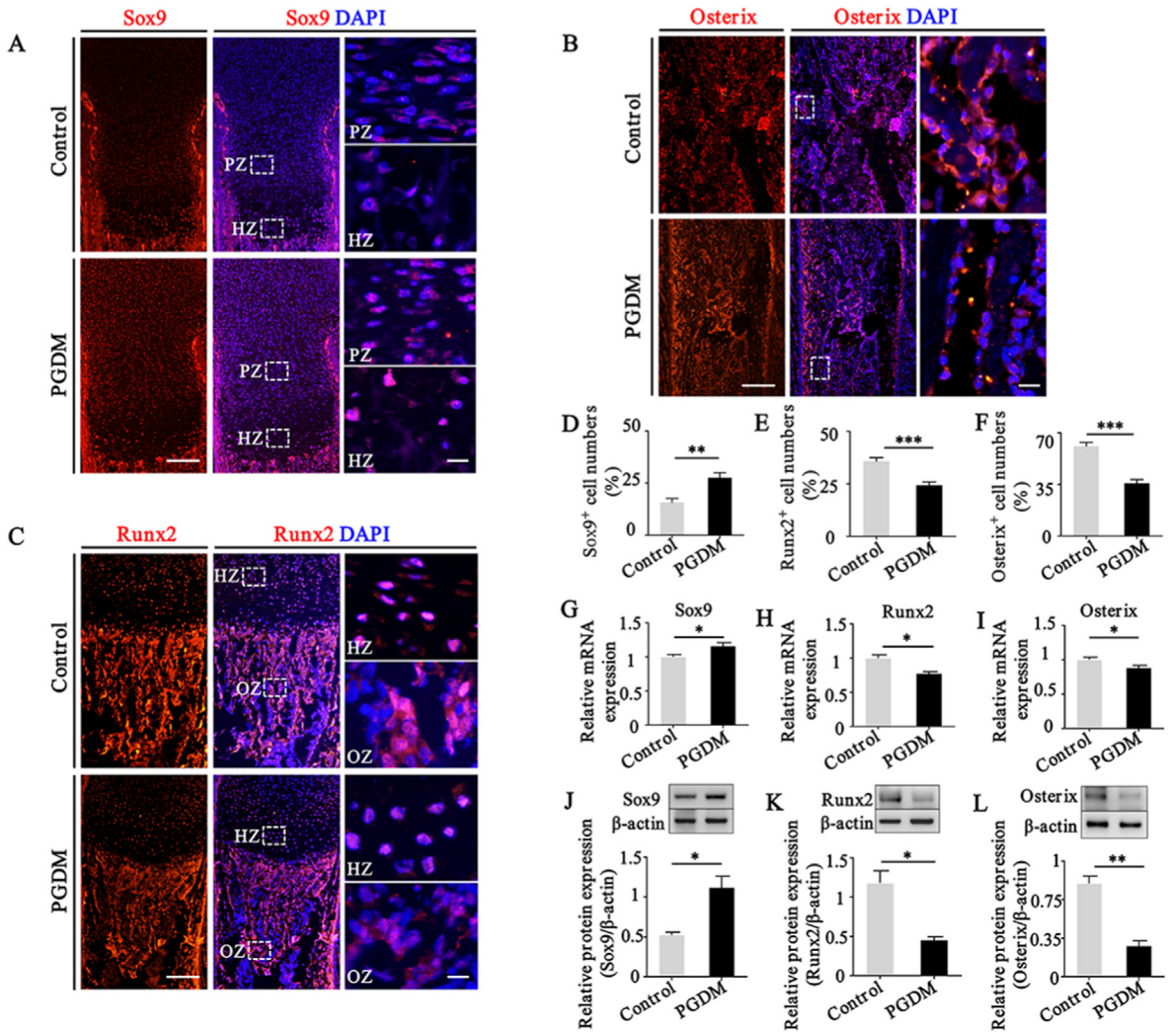

Fig. 2. Assessing the expressions of differentiation-related regulatory genes in the long bone of mouse embryos from control and PGDM group. **A-C**: Representative images of Sox9 (A), Osterix (B) and Runx2 (C) immunofluorescence in the growth plate and diaphysis of E18.5 mouse embryos from control and PGDM group. Cell nuclei were counterstained with DAPI. Right panels are the high magnification images indicated by dotted squares in the middle panels. **D-F**: Bar charts showing the ratio comparisons of $Sox9^+$ (D), $Runx2^+$ (E) and $Osterix^+$ (F) cell numbers of E18.5 mouse embryos from control and PGDM groups. **G-I**: Quantitative PCR data showing the mRNA expression of Sox9 (G), Runx2 (H) and Osterix (I) from E18.5 control and PGDM mouse embryos. **J-L**: Western blot data showing the expression of Sox9 (J), Runx2 (K) and Osterix (L) from E18.5 control and PGDM mouse embryos. Scale bars = 400 μm in the left and middle panels of A-C, 50 μm in the right panels of A-C. For D, n = 9, for E, n = 7, for F, n = 6, for G-I, n = 3. $^*P < 0.05$, $^{**}P < 0.01$, $^{***}P < 0.001$.

monoclonal primary antibodies against: Sox9 (1:200, Abcam, ab3697, Cambridge, MA), Runx2 (1:200, Abcam, ab114133, USA), Osterix (1:300, Abcam, ab22552, UK), Bmp2 (1:100, Santa Cruz Biotechnology, sc137087, USA), Phospho-p38 (1:200, Cell Signaling Technology, #9211, USA), IκBα (1:200, Cell Signaling Technology, #4814, Boston, MA), p50 (1:100, Bioss, bs-1194 R, USA), p65 (1:200, Cell Signaling Technology, SA), Phospho-p65 (1:100, Cell Signaling Technology, #3033, Boston, USA). The secondary antibody, Alexa Fluor 555 anti-rabbit IgG (1:1000, Invitrogen, CA, USA) or Alexa Fluor 488 anti-rabbit IgG (1:1000, Invitrogen, CA, USA), was then applied. The sections were counter-stained with 4′-6-diamidino-2-phenylindole (DAPI, 5 μg/mL, Life Tech, USA) to reveal the nuclei and finally photographed by an Olympus IX51 microscope (Olympus, Tokyo, Japan). The immunofluorescent intensity was quantitative measured as previously described [37,38]. The results were analyzed using IPP 5.0 or image J software. Negative controls of the immunofluorescent staining were attached as supplementary figure 1 and 2 (Fig. S1-S2).

2.6. RNA isolation and quantitative PCR

Total RNA was extracted from the harvested mouse femoral head and ATDC5 cells using a Trizol kit (Invitrogen, Waltham, MA, USA). RNA (1 μg) was reverse transcribed, using 1 μL Oligo dT, 1 μL StarScript II RT mix, primer, and 10 μL 2 × reaction mix, according to the manufacturer's instructions (Genstar, Beijing, China). First-strand cDNA (0.4 μL) was synthesized to a final volume of 20 μL using a SuperScript RIII first-strand kit (Invitrogen, Waltham, MA, USA). Following reverse transcription, PCR amplification of the cDNA was performed using mouse specific primers. The primers' sequences are provided in Table 1. The PCR reactions were performed in a Bio-Rad S1000TM Thermal cycler (Bio-Rad, Hercules, CA, USA) as described previously [39]. The expression of the genes was normalized to β-actin, and the expression levels were compared by ΔΔCt. The quantitative PCR results shown are the representative of three independent experiments.

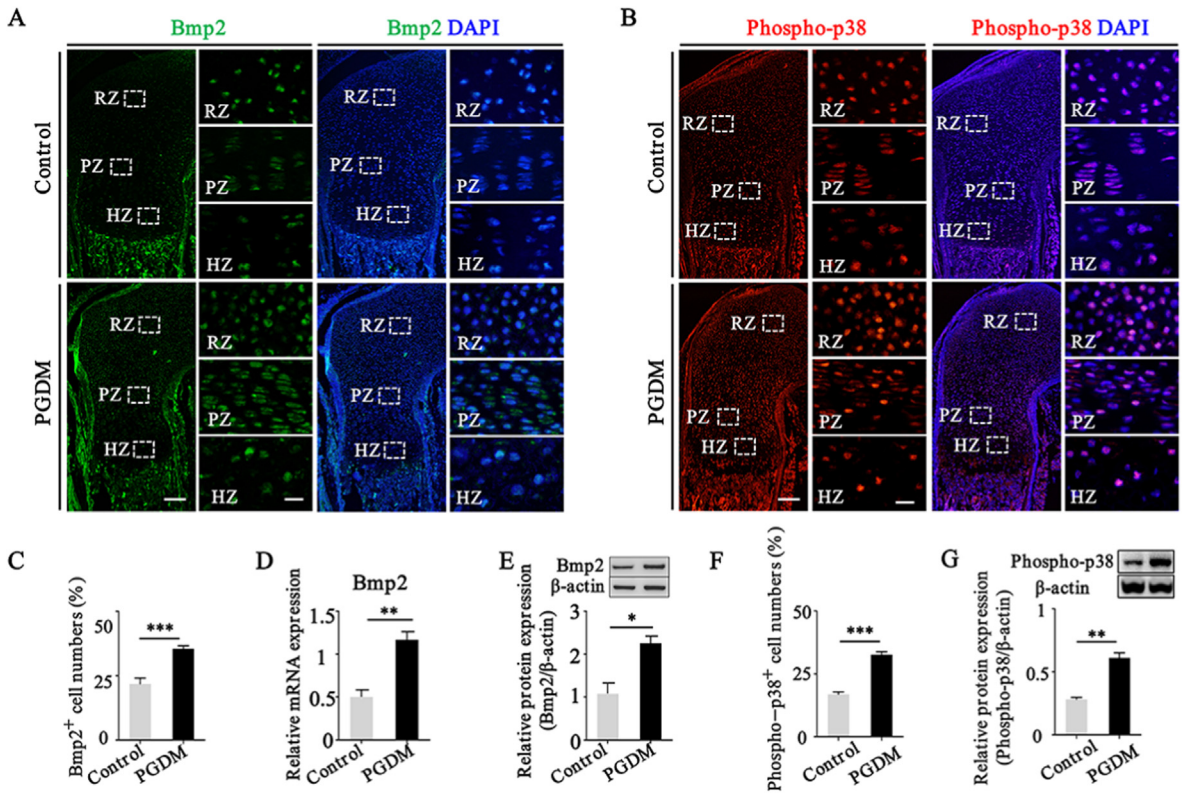

Fig. 3. Assessing the expressions of Bmp2 signaling in the growth plate of mouse embryos from control and PGDM group. **A-B**: Representative images of Bmp2 (A) and Phospho-p38 (B) immunofluorescence in the growth plate of E18.5 mouse embryos from control and PGDM group. Cell nuclei were counterstained with DAPI. The second and fourth panels are the high magnification images indicated by dotted squares in the first and third panels, respectively. **C, F**: Bar charts showing the ratio comparisons of $Bmp2^+$ (C) and $Phospho\text{-}p38^+$ (F) cell numbers of E18.5 mouse embryos from control and PGDM groups. **D**: Quantitative PCR data showing the mRNA expression of Bmp2 from E18.5 control and PGDM mouse embryos. **E, G**: Western blot data showing the expression of Bmp2 (E) and Phospho-p38 (G) from E18.5 control and PGDM mouse embryos. Scale bars = 400 μm in the first and third panels of A-B, 50 μm in the second and fourth panels of A-B. For C and F, n = 18, for D, E and G, n = 3. $^*P < 0.05$, $^{**}P < 0.01$, $^{***}P < 0.001$.

2.7. Western blotting

Proteins derived from the femoral head of the mouse embryos and ATDC5 cells were isolated using a radio-immuno-precipitation assay buffer (RIPA, Sigma–Aldrich, St. Louis, MO, USA). The concentration of protein was quantified with a BCA assay (Thermo Fisher Scientific, Waltham, MA, USA). The extracted protein was separated by 10% SDS-PAGE and transferred onto a polyvinylidene difluoride (PVDF) membrane (Millipore, MA, USA). The membrane was blocked with 5% nonfat milk and then incubated with Bmp2 (1:500, Santa Cruz Biotechnology, sc137087, USA), Phospho-p38 (1:1000, Cell Signaling Technology, #9211, USA), p65 (1:1000, Cell Signaling Technology, SA) and β-actin (1:3000; Proteintech, 60008-1-1 g, Rosemont, USA) in a TBST buffer at 4 °C overnight. After incubation with the secondary antibody, either HRP goat anti-rabbit IgG (1:3000; EarthOx, 7074 S, Millbrae, USA) or HRP goat anti-mouse IgG (1:3000; EarthOx, 7076 S, Millbrae, USA), the samples were developed with SuperSignalTM West Femto Chemiluminescent Substrate (ThermoFisher, Rockford, USA) and the Gel Doc™ XR + System (Bio-Rad, CA, USA). Quantity One (Bio-Rad, Hercules, CA, USA) was used to capture the chemiluminescent signals and analyze the data. All samples were performed in triplicate.

2.8. Data analysis

Statistical analysis was performed using SPSS 22.0 statistical package program. Constructions of statistical charts were performed using a Graphpad Prism 5 software package (Graphpad Software, CA, USA). Data were presented as means ± SD. All data were analyzed using ANOVA and *t* text, which were employed to establish whether there was any significant difference between the control and experimental data. $P < 0.05$ was considered statistically significant.

3. Results

3.1. Hyperglycemia during pregnancy suppresses the development of long bones in mouse fetus through influencing on the growth plate

In order to evaluate the effect of PGDM on the embryonic long bone formation, we established the mouse model of PGDM via intraperitoneal injection of STZ as shown in Fig. 1A. Compared to the control, the crown-rump length and body weights of PGDM mouse embryos were significantly reduced (Fig. 1B–E). Alcian blue/alizarin red staining showed that the lengths of humerus, radius, ulna, femur, fibula and tibia of E18.5 PGDM mouse embryos were significantly shorter than the ones of control embryos (Fig. 1F–I). H&E staining on longitudinal sections of the femur demonstrated that there were no significant difference on the proportion of rest zone (RZ) and proliferative zone (PZ) to the entire length of growth plate between control and PGDM mouse embryos, but there was a significant increase on the proportion of growth plate to the entire femur length and hypertrophic zone (HZ) to the entire growth plate in PGDM group when compared to control mouse embryos (Fig. 1J-M).

We further examined the expressions of Sox9 and Runx2, the two crucial transcription factors determining the cell fate of osteochondral progenitors into either chondrocytes or osteoblasts [40], in the long bones of E18.5 mouse embryos, using immunofluorescence, quantitative PCR and western blot. The results displayed that Sox9 expression was significantly increased in the growth plates of E18.5 PGDM mouse embryos (Fig. 2A, D, G, J), while the expression of Runx2 were significantly

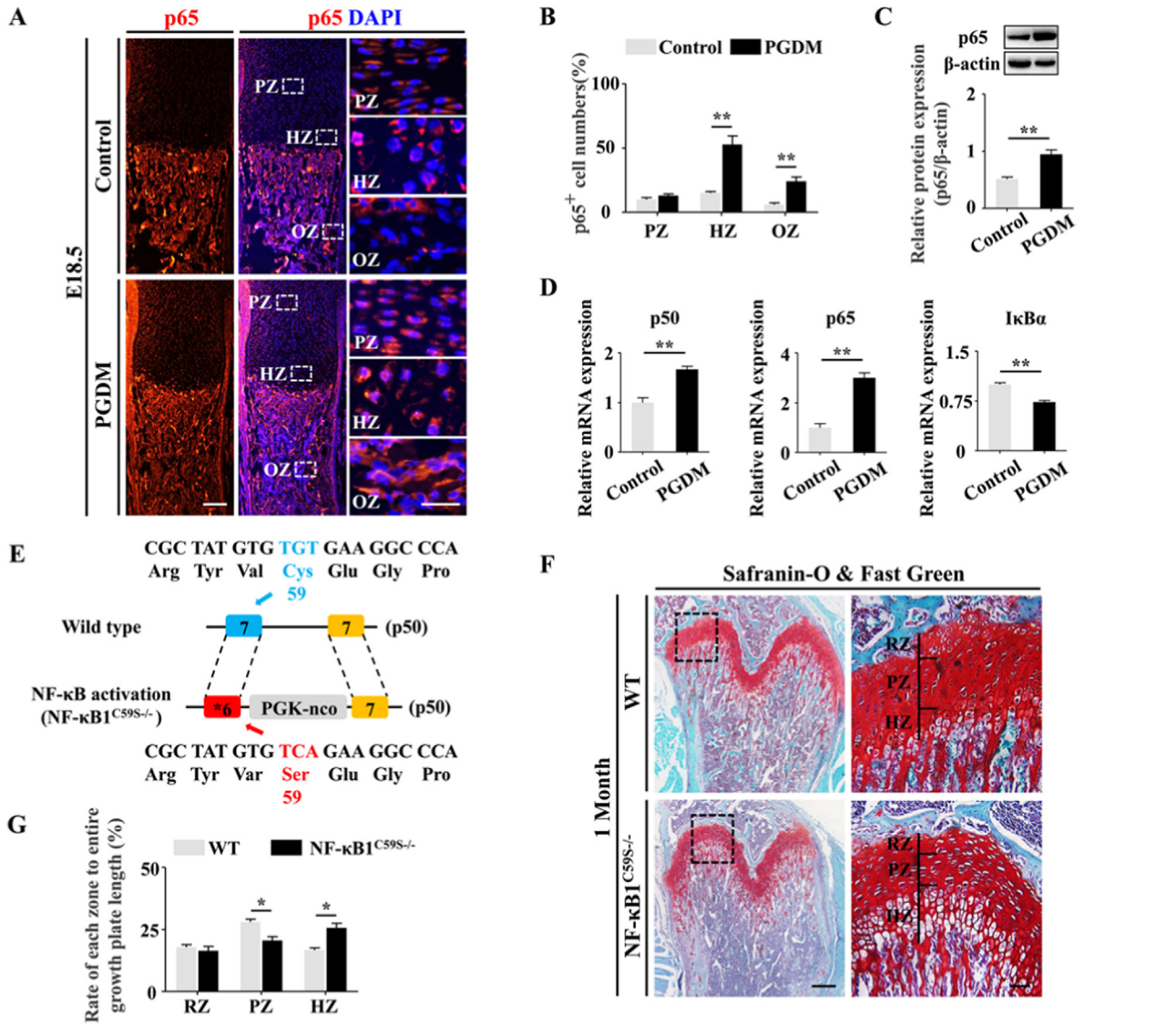

Fig. 4. Assessing the expressions of NF-κB signaling molecules in the long bone of mouse embryos from control and PGDM group. **A**: Representative images of p65 immunofluorescence in the long bones of E18.5 control and PGDM mouse embryos. Cell nuclei were counterstained with DAPI. Right panels are the high magnification images indicated by dotted squares in the middle panels. **B**: Bar charts showing the ratio comparisons of $p65^+$ cell numbers in PZ, HZ and OZ (ossification zone) of the femur of E18.5 mouse embryos from control and PGDM group. **C**: Western blot data showing the expression of p65 from E18.5 control and PGDM mouse embryos. **D**: Quantitative PCR data showing the mRNA expression of p50, p65 and IκBα from E18.5 mouse embryos of control and PGDM group. **E**: Sketch illustrating the NF-κB transgene mice in which NF-κB signaling is activated through altering NF-κB1 (p50) sequence of bases on sixth exon. **F**: Representative images of Safranin-O & Fast Green staining in growth plates of 1-month control and active NF-κB mice. Right panels are the high magnification images indicated by dotted squares in the left panels. **G**: Bar chart showing the comparisons of the ratios of each zone (RZ, PZ, and HZ) to the entire growth plate lengths of 1-month control and active NF-κB mice. Scale bars = 400 μm in the left and middle panels of A, 100 μm in the right panels of A; and 500 μm in the left panels of F, 100 μm in the right panels of F. For B, n = 6, for C and D, n = 3, for G, n = 5. $^*P < 0.05$, $^{**}P < 0.01$.

reduced (Fig. 2C, E, H, K) compared to control ones. Moreover, the expression of Osterix, another key regulator of osteoblasts differentiation and function, exhibited the same tendency as that of Runx2 (Fig. 2B, F, I, L). Taken together, these results suggest that hyperglycemia exposure suppress the transition of hypertrophic chondrocytes and the turnover from HZ to ossification zone (OZ) in growth plate, which subsequently inhibit the development of fetal long bones.

3.2. Bmp2 signaling mediated by NF-κB is involved in the suppression of the turnover from HZ to OZ in PGDM mouse embryos

Previous studies suggested that Sox9 played an important role in the regulation of chondrocyte hypertrophic maturation and ossification [41], and the persistent expression of Sox9 retarded the transdifferentiation of chondrocytes into osteoblasts at the cartilage–bone junction [42]. Bmp2, judged as the upstream signaling of Sox9 [43], might be involved in the up-regulation of Sox9. Therefore, we next measured the expression of Bmp2 and downstream Phospho-p38 in E18.5 mouse embryonic growth plates using immunofluorescent staining. The results showed that both Bmp2 (Fig. 3A, C) and Phospho-p38 expressions (Fig. 3B, F) were significantly increased in the growth plate of PGDM mouse embryos compared to control ones, which was further confirmed by the data of quantitative PCR and western blot (Fig. 3D–E, G).

It was reported that the expression of Bmp2 was partially controlled by NF-κB in chondrocytes, which may have important impacts in late stage chondrogenesis [30]. So the expression of p65, the marker of NF-κB signaling, was checked in E18.5 mouse embryos growth plates using immunofluorescent staining. The results showed that p65 expression was

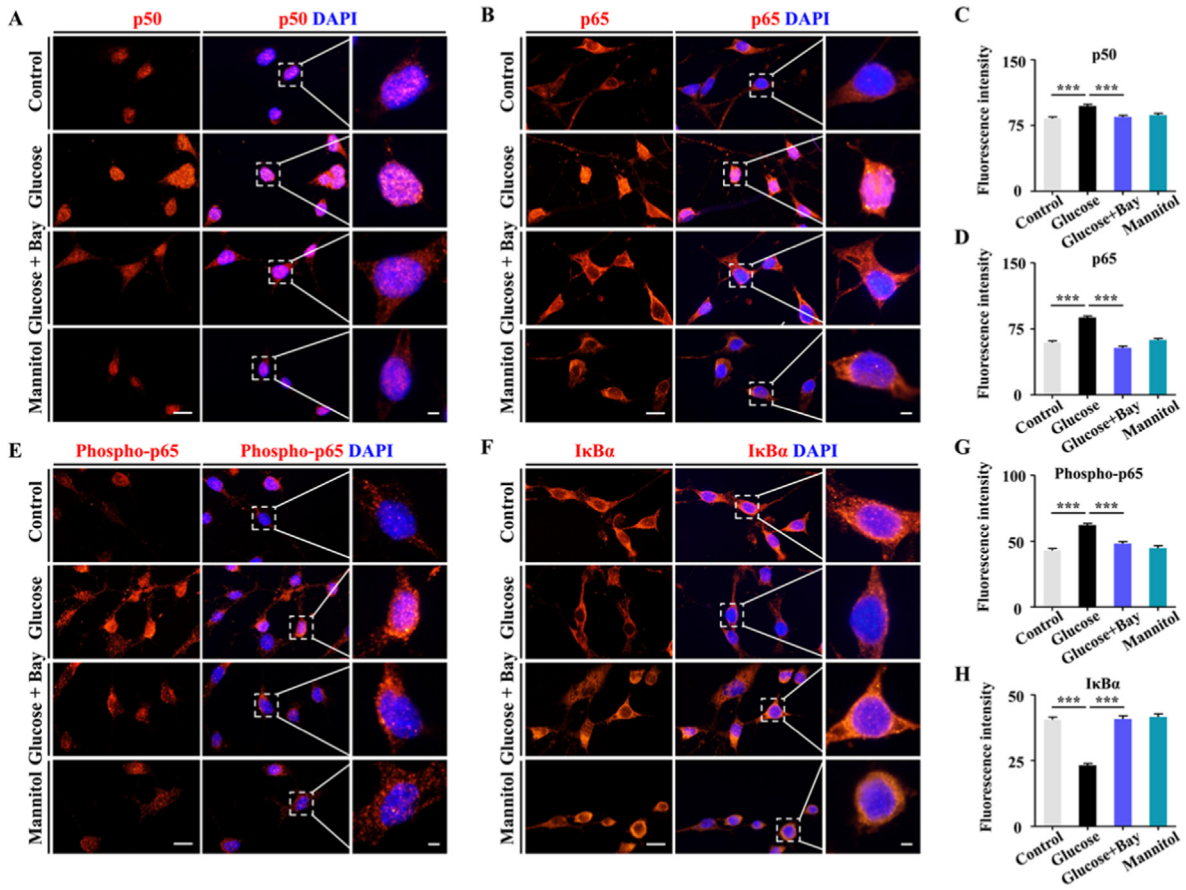

Fig. 5. Assessing the expressions of NF-κB signaling in chondrogenic ATDC5 cells in the presence of high concentration of glucose or blocking NF-κB signaling. **A-B, E-F**: Representative expressions of p50 (A), p65 (B), Phospho-p65 (E), IκBα (F) using immunofluorescence in ATDC5 cells from control, glucose, and glucose + bay groups. Mannitol was used as osmotic control. Cell nuclei were counterstained with DAPI. Right panels are the high magnification images indicated by dotted squares in the middle panels. **C-D, G-H**: Bar charts showing the comparisons of relative fluorescence intensities of p50 (C), p65 (D), Phospho-p65 (G), IκBα (H) in ATDC5 cells from control, glucose, glucose + bay and mannitol groups. Scale bars = 50 μm in the left and middle panels of A, B, E and F, 10 μm in the right panels of A, B, E and F. For C, D, G and H, n = 50. $^{***}P < 0.001$.

increased in the growth plate of PGDM mouse embryos compared to control ones (Fig. 4A and B), especially in HZ and OZ, which was confirmed by quantitative PCR and western blot data (Fig. 4C and D). The possibility is that hyperglycemia exposure activates NF-κB molecules, which subsequently increase the expressions of Bmp2 and Sox9. To verify the speculation, a NF-κB activated transgenic mice, NF-κB1^{C59S}, was employed in this experiment (Fig. 4E) to address the effect of NF-κB on the development of growth plate. The rate of each zone to the entire growth plate in the NF-κB activated mice were quantitatively compared with the ones in wild-type mice. The results showed that the ratio of HZ to the entire growth plate length was significantly increased when compared with the wild type mice, exhibiting the same phenotype as that of the PGDM mouse embryos (Fig. 4F and G). Also, the expressions of Sox9, Runx2 and Osterix were checked in the growth plate of the femur of the NF-κB1^{C59S} mice using immunofluorescence. The results displayed that the expressive pattern of above-mentioned genes exhibited the same tendency as those expressed in the long bones of the E18.5 PGDM mouse embryos (Fig. S3).

Next, ATDC5 cells were employed in vitro to verify the role of NF-κB on the expression of chondro-osteogenic markers, Sox9 and Runx2. Firstly, immunofluorescent staining manifested that blocking NF-κB signaling with its inhibitor, Bay-117082, would reverse the increases of high glucose-induced p50 (Fig. 5A, C), p65 (Fig. 5B, D) and Phospho-p65 (Fig. 5E, G) expressions in ATDC5 cells, while the inhibited IκBα immunofluorescence intensity induced by high glucose was significantly increased by blocking NF-κB signaling (Fig. 5F, H) in ATDC5 cells. Furthermore, the immunofluorescence revealed that high glucose elevated Bmp2 (Fig. 6A, C), Phospho-p38 (Fig. 6B, D), Sox9 (Fig. 6E, G) and inhibited Runx2 (Fig. 6F, H) expressions in ATDC5 cells, which could be reversed by the addition of Bay-117082 (Fig. 6).

4. Discussion

The formation of long bones in the vertebrates adopts endochondral ossification, in which bone gradually replaces the previous cartilage template [44]. GH-IGF axis, a mixed system of endocrine, paracrine and autocrine, is deemed to primarily plays an indispensable role on longitudinal bone growth [45]. Uchimura et al. reported that IGF2 regulated bone growth via influencing glucose metabolism in chondrocytes, indicating the role of glucose metabolism on cartilage development [46]. The risk of skeletal mass loss and impairment of bone development were described in the children with diabetes [47]. Weiss et al. reported that STZ-induced diabetes influenced on the stages of matrix-induced endochondral bone growth of the rats, which are derived from the following mechanism of action: the suppression of mesenchymal cell proliferation; the reduction of vascular invasion during osteogenesis; and the regression of calcification and ossification [48]. In this study, we also found the restriction of mouse endochondral bone growth as shown above, and assumed that the principal mechanism was the accumulation of hypertrophic chondrocytes, i.e., the relatively expanded HZ, in HZ of growth plate (Fig. 1). The abnormity of terminal differentiation of hypertrophic chondrocytes held a clue to the possible causes of aberrant turnover of

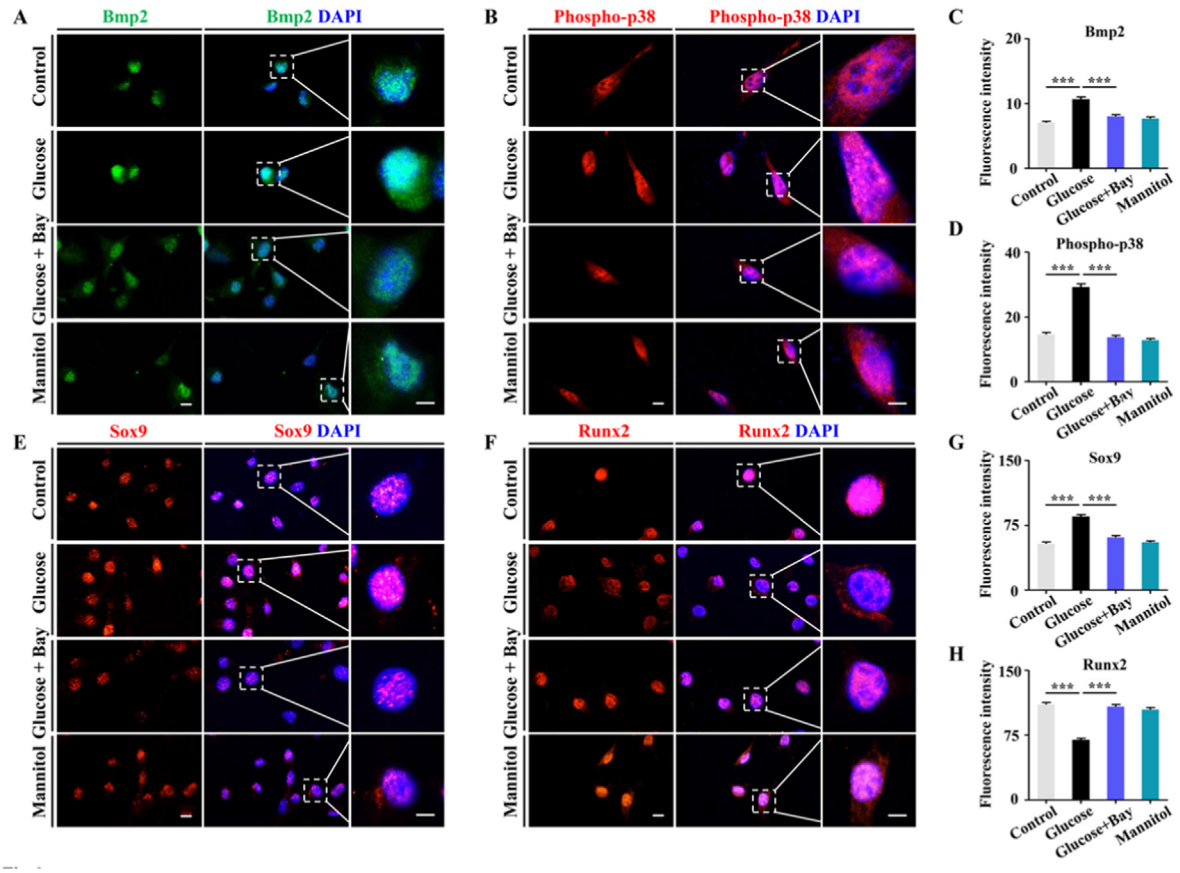

Fig. 6. Assessing the expressions of differentiation-related regulatory genes in ATDC5 cells in the presence of high concentration of glucose or blocking NF-κB signaling. **A-B, E-F**: Representative expressions of Bmp2 (A), Phospho-p38 (B), Sox9 (E) and Runx2 (F) using immunofluorescence in ATDC5 cells from control, glucose, glucose + bay, and mannitol groups. Cell nuclei were counterstained with DAPI. Right panels are the high magnification images indicated by dotted squares in the middle panels. **C-D, G-H**: Bar charts showing the comparisons of relative fluorescence intensities of Bmp2 (C), Phospho-p38 (D), Sox9 (G) and Runx2 (H) in ATDC5 cells from control, glucose, glucose + bay, and mannitol groups. Scale bars = 50 μm in the left and middle panels of A, B, E and F, 10 μm in the right panels of A, B, E and F. For C, D, G and H, n = 50. ***$P < 0.001$.

hypertrophic chondrocytes at growth plate, i.e., the disruption of growth plate homeostasis under certain circumstances. This was partially verified by the alteration of Sox9 and Runx2 expression in the growth plate of PGDM mouse embryos in this study (Fig. 2), since Sox9 is deemed to dominantly regress the activity of Runx2 for destining chondrogenic lineage in the process of endochondral ossification [49]. Meanwhile, in PGDM mouse embryos, we also observed the reduction of the Osterix expression in the long bones (Fig. 2). Osterix acts as a downstream signaling molecule of Runx2 and plays an important role on preosteoblast development during osteogenesis [50], and the reduction of Osterix expression in growth plate would contribute to the turnover barrier of osteochondrogenic progenitors from hypertrophic zone to ossification zone.

Next question is how diabetes mellitus negatively affect the endochondral bone formation through influencing the normal transformation of osteochondrogenic progenitors from hypertrophic zone to ossification zone. As well known, diabetes mellitus is closely associated with the activation of NF-κB signaling pathway, which functions as a key event in the pathological mechanisms of diabetes mellitus [51–53]. Likewise, we indeed found that NF-κB signaling activation existed in the growth plate of PGDM mouse embryos in this study (Fig. 4). More interestingly, we correspondingly observed the phenotype of the extended hypertrophic zone in the transgenic mice of activation of NF-κB signaling (Fig. 4), which is similar to the growth plate established in PGDM mouse embryos. Furthermore, we discovered that the activation of NF-κB signaling in ATDC5 cells induced by high glucose could be successfully reversed by blocking NF-κB signaling with its inhibitor (Fig. 5). And inhibiting the activation of NF-κB also decreased the expression of Bmp2, Phospho-p38 and Sox9 caused by high glucose exposure, as well as restored the down-regulation of Runx2 (Fig. 6). These results indicated the role of key mediator of NF-κB signaling between maternal environment of diabetes mellitus and initial bone formation during embryonic development. Taken together, the data enforced and confirmed that NF-κB signaling was indeed involved in the pathobiology of diabetes-induced endochondral bone formation.

The question then is how the activated NF-κB signaling lead to the possibility of abnormal bone formation due to the problem of chondrogenic differentiation as described above. Previous study reported that NF-κB specifically activates Bmp2 gene expression in growth plate chondrocytes in vivo and in a chondrocyte cell line in vitro [30], while the latter, as the upstream signal of Sox9, subsequently up-regulates the expression of Sox9. In this study, we certainly manifested the increase of Bmp2, Phospho-p38 and Sox9 expression in ATDC5 cells from the high glucose-induced repressive state in the context of blocking NF-κB signaling with its inhibitor (Fig. 6).

In sum (Fig. 7), we revealed the possible pathological mechanism of diabetes-induced the restriction of trans-differentiation of chondrocytes from hypertrophic zone to bone cells in the ossification zone in the present study. Briefly, the hyperglycemia in diabetes mellitus induced Bmp2/Phospho-p38 expression through the mediation effect of activated NF-κB signaling, and Bmp2 increased the expression of Sox9 (the crucial transcription factor for early chondrogenesis) in growth plate. Thus, the enhanced Sox9 in turn inhibited the expressions of Runx2 and Osterix, which functions as the master osteogenic factors. Eventually, these would

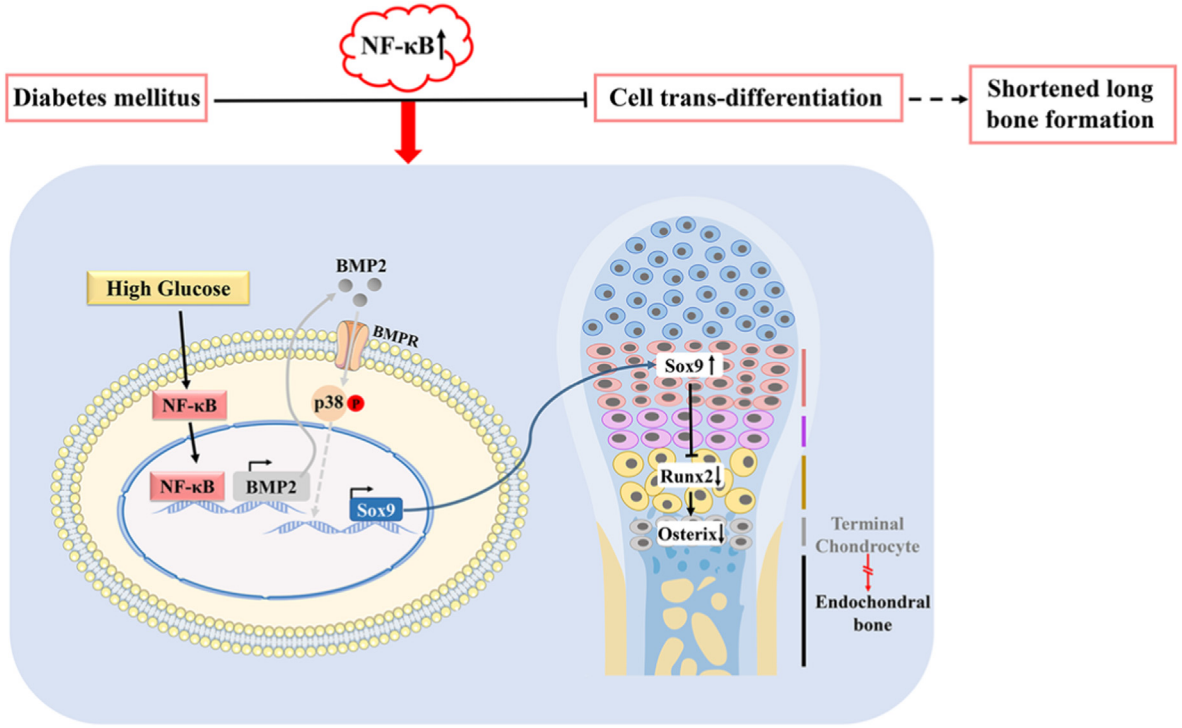

Fig. 7. Schematic diagram of the proposed mechanism about high glucose disturbed the trans-differentiation from hypertrophic chondrocytes to bone cells in the ossification zone through the mediation effect of NF-κB-Bmp2 signaling.

restrict the trans-differentiation of chondrocytes/bone cells relay from hypertrophic zone to ossification zone, and subsequently result in the shortened long bones. It is expected the exact biological mechanisms will be further addressed, to combat diabetic complications on fetal skeletal development in the future.

Declaration of competing interest

The authors declared that there are no conflicts of interests.

Acknowledgments

This study was supported by Natural Science Foundation of Guangdong Province (2020A1515010209, 2021A1515012393), NSFC grant (31971108 and 31771331), Fundamental Research Funds for the Central Universities (21621106). We would like to thank Medical experimental center in Jinan University.

Appendix A. Supplementary data

Supplementary data to this article can be found online at https://doi.org/10.1016/j.jot.2021.10.009.

References

[1] Chen L, Magliano DJ, Zimmet PZ. The worldwide epidemiology of type 2 diabetes mellitus—present and future perspectives. Nat Rev Endocrinol 2012;8(4):228–36.
[2] Seino Y, Nanjo K, Tajima N, Kadowaki T, Kashiwagi A, Araki E, et al. Report of the committee on the classification and diagnostic criteria of diabetes mellitus. Diabetol Int 2010;1(1):2–20.
[3] Xiang AH, Wang X, Martinez MP, Getahun D, Page KA, Buchanan TA, et al. Maternal gestational diabetes mellitus, type 1 diabetes, and type 2 diabetes during pregnancy and risk of ADHD in offspring. Diabetes Care 2018;41(12):2502–8.
[4] Bánhidy F, Ács N, Puhó EH, Czeizel AE. Congenital abnormalities in the offspring of pregnant women with type 1, type 2 and gestational diabetes mellitus: a population-based case-control study. Congenital Anom 2010;50(2):115–21.
[5] Mackin ST, Nelson SM, Kerssens JJ, Wood R, Wild S, Colhoun HM, et al. Diabetes and pregnancy: national trends over a 15 year period. Diabetologia 2018;61(5):1081–8.
[6] Casey BM, Lucas MJ, McIntire DD, Leveno KJ. Pregnancy outcomes in women with gestational diabetes compared with the general obstetric population. Obstet Gynecol 1997;90(6):869–73.
[7] Xiong X, Saunders L, Wang F, Demianczuk N. Gestational diabetes mellitus: prevalence, risk factors, maternal and infant outcomes. Int J Gynecol Obstet 2001;75(3):221–8.
[8] Barahona MJ, Sucunza N, García-Patterson A, Hernández M, Adelantado JM, Ginovart G, et al. Period of gestational diabetes mellitus diagnosis and maternal and fetal morbidity. Acta Obstet Gynecol Scand 2005;84(7):622–7.
[9] Jensen DM, Sørensen B, Feilberg-Jørgensen N, Westergaard J, Beck-Nielsen H. Maternal and perinatal outcomes in 143 Danish women with gestational diabetes mellitus and 143 controls with a similar risk profile. Diabet Med 2000;17(4):281–6.
[10] Retzepi M, Donos N. The effect of diabetes mellitus on osseous healing. Clin Oral Implants Res 2010;21(7):673–81.
[11] Jiao H, Xiao E, Graves DT. Diabetes and its effect on bone and fracture healing. Curr Osteoporos Rep 2015;13(5):327–35.
[12] Namgung R, Tsang RC. Bone in the pregnant mother and newborn at birth. Clin Chim Acta 2003;333(1):1–11.
[13] Eriksson U, Dahlstrom E, Larsson KS, Hellerstrom C. Increased incidence of congenital malformations in the offspring of diabetic rats and their prevention by maternal insulin therapy. Diabetes 1982;31(1):1–6.
[14] Banerjee S, Ghosh US, Banerjee D. Effect of tight glycaemic control on fetal complications in diabetic pregnancies. J Assoc Phys India 2004;52:109–13.
[15] Suhonen L, Hiilesmaa V, Teramo K. Glycaemic control during early pregnancy and fetal malformations in women with type I diabetes mellitus. Diabetologia 2000;43(1):79–82.
[16] Done SL. Fetal and neonatal bone health: update on bone growth and manifestations in health and disease. Pediatr Radiol 2012;42(1):158–76.
[17] Jing Y, Wang Z, Li H, Ma C, Feng J. Chondrogenesis defines future skeletal patterns via cell transdifferentiation from chondrocytes to bone cells. Curr Osteoporos Rep 2020;18(3):199–209.
[18] Kronenberg HM. Developmental regulation of the growth plate. Nature 2003;423(6937):332–6.
[19] Ornitz DM, Marie PJ. FGF signaling pathways in endochondral and intramembranous bone development and human genetic disease. Gene Dev 2002;16(12):1446–65.
[20] Murakami S, Kan M, McKeehan WL, De Crombrugghe B. Up-regulation of the chondrogenic Sox9 gene by fibroblast growth factors is mediated by the mitogen-activated protein kinase pathway. Proc Natl Acad Sci Unit States Am 2000;97(3):1113–8.
[21] Naski MC, Colvin JS, Coffin JD, Ornitz DM. Repression of hedgehog signaling and BMP4 expression in growth plate cartilage by fibroblast growth factor receptor 3. Development 1998;125(24):4977–88.
[22] Minina E, Kreschel C, Naski MC, Ornitz DM, Vortkamp A. Interaction of FGF, Ihh/Pthlh, and BMP signaling integrates chondrocyte proliferation and hypertrophic differentiation. Dev Cell 2002;3(3):439–49.

[23] Kingsley DM, Bland AE, Grubber JM, Marker PC, Russell LB, Copeland NG, et al. The mouse short ear skeletal morphogenesis locus is associated with defects in a bone morphogenetic member of the TGFβ superfamily. Cell 1992;71(3):399–410.
[24] Shu B, Zhang M, Xie R, Wang M, Jin H, Hou W, et al. BMP2, but not BMP4, is crucial for chondrocyte proliferation and maturation during endochondral bone development. J Cell Sci 2011;124(Pt 20):3428–40.
[25] Kwon SH, Lee TJ, Park J, Hwang JE, Jin M, Jang HK, et al. Modulation of BMP-2-induced chondrogenic versus osteogenic differentiation of human mesenchymal stem cells by cell-specific extracellular matrices. Tissue Eng 2013;19(1–2):49–58.
[26] Iwasaki S, Iguchi M, Watanabe K, Hoshino R, Tsujimoto M, Kohno M. Specific activation of the p38 mitogen-activated protein kinase signaling pathway and induction of neurite outgrowth in PC12 cells by bone morphogenetic protein-2. J Biol Chem 1999;274(37):26503–10.
[27] Kimura N, Matsuo R, Shibuya H, Nakashima K, Taga T. BMP2-induced apoptosis is mediated by activation of the TAK1-p38 kinase pathway that is negatively regulated by Smad6. J Biol Chem 2000;275(23):17647–52.
[28] Raingeaud J, Whitmarsh AJ, Barrett T, Dérijard B, Davis RJ. MKK3- and MKK6-regulated gene expression is mediated by the p38 mitogen-activated protein kinase signal transduction pathway. Mol Cell Biol 1996;16(3):1247–55.
[29] Moriguchi T, Kuroyanagi N, Yamaguchi K, Gotoh Y, Irie K, Kano T, et al. A novel kinase cascade mediated by mitogen-activated protein kinase kinase 6 and MKK3. J Biol Chem 1996;271(23):13675–9.
[30] Feng JQ, Xing L, Zhang JH, Zhao M, Horn D, Chan J, et al. NF-kappaB specifically activates BMP-2 gene expression in growth plate chondrocytes in vivo and in a chondrocyte cell line in vitro. J Biol Chem 2003;278(31):29130–5.
[31] Hayden MS, Ghosh S. Shared principles in NF-κB signaling. Cell 2008;132(3):344–62.
[32] Anest V, Hanson JL, Cogswell PC, Steinbrecher KA, Strahl BD, Baldwin AS. A nucleosomal function for IκB kinase-α in NF-κB-dependent gene expression. Nature 2003;423(6940):659–63.
[33] Chen L-F, Greene WC. Shaping the nuclear action of NF-κB. Nat Rev Mol Cell Biol 2004;5(5):392–401.
[34] Xu JJ, Wang G, Luo X, Wang LJ, Bao Y, Yang X. Role of nuclear factor-κB pathway in the transition of mouse secondary follicles to antral follicles. J Cell Physiol 2019;234(12):22565–80.
[35] Ovchinnikov D. Alcian blue/alizarin red staining of cartilage and bone in mouse. Cold Spring Harb Protoc 2009;2009(3). pdb. prot5170.
[36] Sun Y, Xu J, Xu L, Zhang J, Chan K, Pan X, et al. MiR-503 promotes bone formation in distraction osteogenesis through suppressing Smurf1 expression. Sci Rep 2017;7(1):1–10.
[37] Cheng X, Li PZ, Wang G, Yan Y, Li K, Brand-Saberi B, et al. Microbiota-derived lipopolysaccharide retards chondrocyte hypertrophy in the growth plate through elevating Sox9 expression. J Cell Physiol 2019;234(3):2593–605.
[38] Wang G, Hu YX, He MY, Xie YH, Su W, Long D, et al. Gut-lung dysbiosis accompanied by diabetes mellitus leads to pulmonary fibrotic change through the NF-κB signaling pathway. Am J Pathol 2021;191(5):838–56.
[39] Xu S, Guo R, Li PZ, Li K, Yan Y, Chen J, et al. Dexamethasone interferes with osteoblasts formation during osteogenesis through altering IGF-1-mediated angiogenesis. J Cell Physiol 2019;234(9):15167–81.
[40] Zou L, Zou X, Li H, Mygind T, Zeng Y, Lü N, et al. Molecular mechanism of osteochondroprogenitor fate determination during bone formation. In: Tissue engineering. Springer; 2006. p. 431–41.
[41] Dy P, Wang W, Bhattaram P, Wang Q, Wang L, Ballock RT, et al. Sox9 directs hypertrophic maturation and blocks osteoblast differentiation of growth plate chondrocytes. Dev Cell 2012;22(3):597–609.
[42] Lui JC, Yue S, Lee A, Kikani B, Temnycky A, Barnes KM, et al. Persistent Sox9 expression in hypertrophic chondrocytes suppresses transdifferentiation into osteoblasts. Bone 2019;125:169–77.
[43] Pan Q, Yu Y, Chen Q, Li C, Wu H, Wan Y, et al. Sox9, a key transcription factor of bone morphogenetic protein-2-induced chondrogenesis, is activated through BMP pathway and a CCAAT box in the proximal promoter. J Cell Physiol 2008;217(1):228–41.
[44] Karsenty G, Wagner EF. Reaching a genetic and molecular understanding of skeletal development. Dev Cell 2002;2(4):389–406.
[45] Wit JM, Camacho-Hübner C. Endocrine regulation of longitudinal bone growth. In: Cartilage and bone development and its disorders, vol. 21. Karger Publishers; 2011. p. 30–41.
[46] Uchimura T, Hollander JM, Nakamura DS, Liu Z, Rosen CJ, Georgakoudi I, et al. An essential role for IGF2 in cartilage development and glucose metabolism during postnatal long bone growth. Development 2017;144(19):3533–46.
[47] Ferrari S. Diabetes and Bone. Calcif Tissue Int 2017;100(2):107–8.
[48] Weiss RE, Reddi AH. Influence of experimental diabetes and insulin on matrix-induced cartilage and bone differentiation. Am J Physiol Endocrinol Metabol 1980;238(3):E200–7.
[49] Zhou G, Zheng Q, Engin F, Munivez E, Chen Y, Sebald E, et al. Dominance of SOX9 function over RUNX2 during skeletogenesis. Proc Natl Acad Sci Unit States Am 2006;103(50):19004–9.
[50] Nakashima K, Zhou X, Kunkel G, Zhang Z, Deng JM, Behringer RR, et al. The novel zinc finger-containing transcription factor osterix is required for osteoblast differentiation and bone formation. Cell 2002;108(1):17–29.
[51] Patel S, Santani D. Role of NF-κB in the pathogenesis of diabetes and its associated complications. Pharmacol Rep 2009;61(4):595–603.
[52] Kuzmicki M, Telejko B, Wawrusiewicz-Kurylonek N, Lipinska D, Pliszka J, Wilk J, et al. The expression of genes involved in NF-kB activation in peripheral blood mononuclear cells of patients with gestational diabetes. Eur J Endocrinol 2013;168(3):419–27.
[53] Kuhad A, Chopra K. Attenuation of diabetic nephropathy by tocotrienol: involvement of NFkB signaling pathway. Life Sci 2009;84(9–10):296–301.